

# TEMPORAL BEHAVIOR OF A BOUNDARY LAYER SEPARATION WITHIN A RADIAL VANED DIFFUSER

*A. Marsan*\* – *I. Trébinjac*\*\* – *S. Coste*\* – *G. Leroy*\*

\* Turbomeca, Safran group.  
64511, Bordes, France.

aurelien.marsan@ec-lyon.fr – sylvain.coste@turbomeca.fr – gilles.leroy@turbomeca.fr

\*\* Laboratoire de Mécanique des Fluides et d'Acoustique, UMR CNRS 5509  
École Centrale de Lyon, 69134 Ecully Cedex, France.  
isabelle.trebinjac@ec-lyon.fr

## ABSTRACT

The temporal behavior of a flow separation in the hub-suction side corner of a transonic diffuser is studied thanks to unsteady numerical simulations based on the phase-lagged approach. The validity of the numerical results is confirmed by comparison with experimental unsteady pressure measurements. An analysis of the instantaneous skin-friction pattern and particles trajectories is presented, and highlights the structure of the separation and its temporal behavior. The location of the separation is found to be fixed, in spite of the strongly unsteady flow at diffuser inlet, and corresponds to the one predicted by the steady-state numerical simulations. It can justify the development of a control strategy from steady-state simulations.

## NOMENCLATURE

(U)RANS	(Unsteady) Reynolds Averaged Numerical Simulations
bpf	blade passing frequency
$\Omega$	rotational speed of the impeller
$N_1, N_2$	number of impeller blades, diffuser vanes
$P_t$	total pressure
$p_s$	static pressure
$\overline{p_s}$	time-averaged static pressure
$\dot{m}^{\text{std}}$	standard mass flow rate
$\pi_{\text{stage}}^{\text{st}}$	total-to-static stage pressure ratio. $= p_s^{\text{outlet}} / P_t^{\text{inlet}}$
$C_{p, \text{diffuser}}$	static pressure recovery coefficient of the diffuser. $= (p_s^{\text{outlet}} - p_s^{\text{inlet}}) / (P_t^{\text{inlet}} - p_s^{\text{inlet}})$
$S_{\text{stage}}$	setting ratio of the stage operating point. $= \dot{m}_{\text{std}} / \pi_{\text{stage}}^{\text{st}}$
$T_{DR} = \delta t$	period of the diffuser. $= (2\pi) / (\Omega N_1)$
$S_{SS,1} / F_{SS,1}$	seed / focus number 1, located on the suction side

## INTRODUCTION

When Came (1977) reviewed the achievements of research and design effort in high pressure ratio centrifugal compressors in 1977, the centrifugal compressors stage pressure ratios in production engines were limited to 8, efficiency and surge-margin being unacceptable for higher values. The impeller was also identified as the main source of deficit in isentropic efficiency. Since then, understanding of the impeller flow patterns has been significantly enhanced, and the performances of the impellers have increased in such a way that stage pressure ratio higher than 10 can be reached in present engines.

Today, the efforts now focus on the development of more efficient transonic diffusers, with smaller radial extent and increased static pressure recovery. Several studies have furthermore identified the radial vaned diffuser as the limiting element of the stable operating range at low mass flow rates for

various centrifugal compressors, due to the onset of aerodynamic instability, in the form of rotating stall or surge. The optimization of radial diffusers is then expected to also lead to an increase of the surge margin.

As for axial compressors, and as foreseen by Came, the use of boundary layer suction technique may be an efficient way of improvement. Yet, the only published evaluation of the potential of that technique applied on radial diffusers is given by Raw (1986), and concerns a pipe diffuser manufactured by Pratt & Whitney Canada. The other publications referring to boundary layer suction in radial diffusers being patents, namely of Schonenborn (2001) and Leblanc (2010), that both consider fluid removal on the suction side of the diffuser vanes.

Considering on the one hand the lack of experiences regarding boundary layer suction in radial diffusers and on the other hand the significant improvements achieved thanks to that technique in axial machines (Kerrebrock, 2005), a research program supported by Turbomeca, Safran group, was undertaken at the LMFA, École Centrale de Lyon, in order to investigate the benefits of a boundary layer suction in radial vaned diffusers.

The present paper is the continuation of a previous numerical study of the steady-state flow field within the radial diffuser of a transsonic compressor stage (Marsan *et al.*, 2012), which has revealed the growth of a boundary layer separation in the hub-suction side corner of the diffuser vanes when decreasing the mass flow rate, finally leading to the stall of the diffuser vanes. Thanks to the analysis of the flow topology, and from a steady-state point of view, a fluid removal of 0,3% of the stage mass flow rate through a slot on the hub surface close to the vane suction side has allowed the control of that stall. As a consequence, the numerical stable operating range was significantly extended.

However, it is well-known that the flow at the diffuser inlet is strongly time-dependent. Trébinjac *et al.* (2009) have for example demonstrated the inability of steady-state numerical simulations based on the mixing-plane approach to properly predict the shape of the shock in a diffuser with a supersonic inlet Mach number. Bulot (2010) has shown in the same compressor the existence of pressure waves within the diffuser stage, generated by the moving of the impeller blades in front of the radial diffuser and resulting in an increase of the mixing rate. As a consequence, the boundary layer separations predicted by the unsteady calculations were small-sized compared to the steady-state results. Then, the flow at the inlet of the presently studied diffuser being transonic and the radial gap between impeller outlet and diffuser leading edge being significantly small, the effects of unsteadiness on the compressor stage performances have to be considered in order to evaluate the validity of the boundary layer suction strategy parameters coming from the steady-state analysis.

The aim of that paper is to study the modification of the hub-suction side corner boundary layer separation in the diffuser due to unsteadiness. First, the test case is presented. Then, experimental and numerical performance curves are shown, as well as unsteady pressure measurements within the diffuser stage, ensuring the validity of the time-dependent numerical flow field. The temporal behavior of the hub-suction side corner boundary layer separation in the diffuser is then exposed thanks to an analysis of the instantaneous skin-friction patterns and particle tracking, and linked with the diffuser inlet flow temporal fluctuations.

## TEST CASE

The test case is a centrifugal compressor stage manufactured by TURBOMECA, Groupe Safran, used as a rear compression stage in a helicopter engine. It is composed of a backswept splintered unshrouded impeller a radial vaned diffuser, and an axial diffuser. The axial diffuser is not taken into account in the present study. The absolute flow field at the inlet of the diffuser is transonic.

### Experimental rig

The compressor is mounted in a 400 kW test rig in the DAEP Laboratory of the Institut Supérieur de l'Aéronautique et de l'Espace, in Toulouse, France. More details are available in Domercq (1998). Global stage performance coefficients are computed thanks to conventional measurements,

including steady pressure measurements distributed on the circumference at the impeller inlet, at the middle of vaneless diffuser space, and at the diffuser outlet. As an example, at the middle of the vaneless diffuser, an annular chamber is connected to the diffuser vein through 31 holes equally distributed over the circumference. The pressure is measured in this annular chamber. The mass flow rate is measured in the inlet pipe.

A porthole is opened on the entrance area of one of the diffuser vanes, and allows unsteady pressure measurements by using different pierced filling-pavements. Four pavements are available, and allow unsteady pressure measurements at the locations shown in Fig. 1. The unsteady pressure sensors are manufactured by Kulite (reference family XCQ – 093), and were used with their protective grid. Under such conditions, the bandwidth allows to measure the four first harmonics of pressure signal with only 1dB attenuation, and the three next with a 3dB attenuation (Domercq, 1998).

The operating point is set using an automated micrometric discharge valve, controlled in order to reached a prescribed ratio between the mass flow rate and the total-to-static compressor stage pressure ratio. That setting ratio ensures the Mach number and the flow angle to be preserved at the diffuser outlet (Rochuon, 2007).

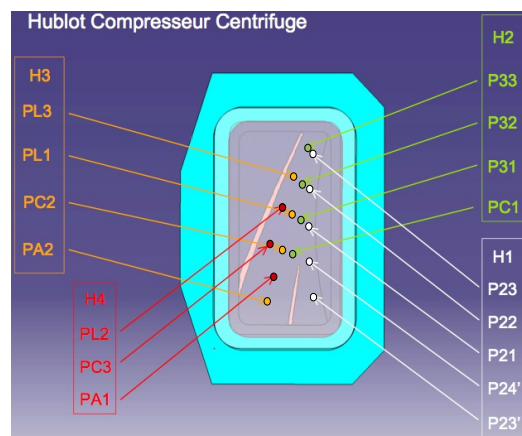


**Fig. 1: Unsteady pressure measurements locations on the four available pavements**

## NUMERICAL PROCEDURE

### Software and turbulence model

Numerical steady and unsteady simulations have been performed using the elsA software, developed by ONERA, the French aerospace Laboratory. This code solves the Reynolds-averaged Navier-Stokes equations by a cell-centered finite volume method. The two variables model of turbulence of Smith (k-l) was chosen for this study, since good agreement between experiments and numerical results were obtained by Rochuon (2007) and Bulot (2010) using it. Numerical model is fully turbulent.

### Phase-lagged approach parameters

For unsteady simulations, the phased-lag approach was used in order to reduce the computational domain to one single passage per row, thanks to the hypothesis of (a) geometrical uniformity of the rows and (b) synchronization of all unsteadiness with the impeller blades passing frequency. Under such conditions, there is only a phase difference between the flow fields in two adjacent passages. Note however that even though these hypothesis are much less restrictive than those of the mixing-plane approach, they don't allow to simulate any aerodynamic instability as rotating stall for example, and may stabilize the boundary layer separations near surge. More details about the phase-lagged technique are given in Neubauer (2004).

The time step is set as a fraction of the smallest temporal period of interaction between the impeller and the diffuser. The dividing factor is designed as  $nqo$ , and is progressively increased from 40 up to 160 during the computation of an operating point. A further decrease in the time-step value has no more influence on the numerical results after  $nqo=160$ . This value depends on the simulated case, but is consistent with previous works (Bulot, 2010).

$$\delta t = \frac{1}{nqo} \times \frac{2\pi}{\Omega N_1 N_2}, \quad nqo \rightarrow 160 \quad [1]$$

At the computational domain boundaries, the temporal flow field is stored thanks to a Fourier transformation relative to the periodicity of the concerned row. The boundary conditions for the next computation step can thus be calculated. The harmonics in each row are stored up to a rank corresponding to 3 times the frequency of the impeller-diffuser phase-lagged interaction [2].

$$f_{harm,max} = 3 \times \frac{\Omega N_1 N_2}{2\pi} \quad [2]$$

### Outlet boundary condition

The outlet boundary condition is set using the setting ratio previously discussed between the value of the static pressure and the mass flow rate, taken at the mesh exit section. The value of the outlet static pressure thus evolves following the relation [3].

$$[p_s]^{(n+1)} = [p_s]^{(n)} \times \left( 1 + \Lambda \times \left[ \frac{[p_s / \dot{m}]^{(n)}}{[p_s / \dot{m}]^{(ref)}} - 1 \right] \right), \quad \Lambda \in [0; 1] \quad [3]$$

This technique, in comparison with a classical simple prescription of the outlet static pressure, allows modeling the flow in the compressor stage beyond the peak of the compressor characteristic. That is necessary in order to study the limit of a compressor operating range, as pointed out by Hill (2007).

### Stage mesh

H, C and O topologies are employed to create a structured multiblocks mesh with the commercial meshing software Numeca Autogrid. The complete mesh is composed of 25 blocks, 18 of which describing the impeller geometry, and 7 the diffuser. The tip clearance is meshed with a O-H topology, in order to ensure a matching connection with the C-mesh block around the impeller blade and the H behind its trailing edge. As for the vane of the diffuser, it is rounded by a O-block. The number of points in the impeller tip clearance height is 21. Fillets are not included, and that could be the point for some future extension of study since they may modify the internal topology of the low-momentum flow area in the hub-suction side diffuser vane corner. The cell width at walls is set to 1  $\mu\text{m}$ . That corresponds to a  $y^+$  parameter approximately equal to 1 along all solid surfaces.

Table 1 exposes the main dimensions of the meshes, the H-blocks upstream of the impeller and downstream of the diffuser being not taken into account. The total mesh is composed of 6,07 millions points.

	Impeller passage	Diffuser passage coarser / normal / refined
meridional direction	217	73 / 141 / 277
tangential direction	137	37 / 81 / 153
height direction	81	65 / 77 / 89

Table 1: Mesh dimensions without upstream and downstream H-blocks

For unsteady computations, the refinement of the impeller and diffuser meshes in the azimuthal direction have to be of the same order of magnitude in order to ensure the suitable transmission of the static pressure waves between the impeller and the diffuser. That leads to some difficulties since meshes are generally more refined in the leading and trailing edge areas, and it was necessary to refine the mesh in the impeller domain in comparison to the one used for steady-state calculations, in order to ensure the continuity of the flow through the impeller-diffuser interface.

Fig. 2 shows a snapshot of the mesh employed for the present study, at the impeller-diffuser interface. The impeller and the diffuser stage meshes are disposed in the critical position from a refinement matching point of view, i.e. the trailing edge of one of the impeller blade is in front of one of the diffuser passage, and the leading edge of the diffuser vane is in front of one of the impeller passage. In that position, about 30 cells of the impeller mesh correspond to one cell of the diffuser mesh at the impeller trailing edge. As for the diffuser leading edge, 8 cells of the diffuser mesh correspond to 1 cell in the impeller.

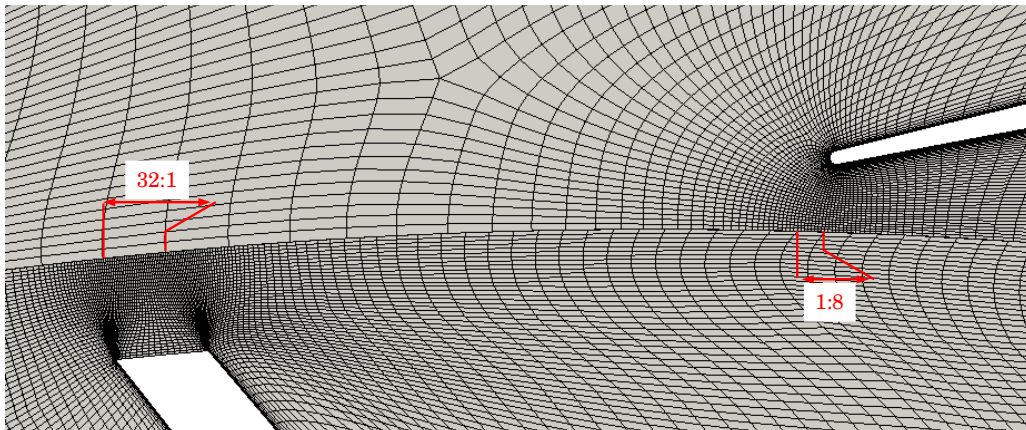


Fig. 2: Comparison of meshes refinements at the impeller-diffuser interface critical ratios of (impeller cells : diffuser cells) in trailing and leading edge areas

## RESULTS AND DISCUSSION

### Validation of numerical results

In this section, the numerical results are compared to the experimental data available, in order to ensure their relevance.

Fig. 3 shows the total-to-static pressure ratio of the compressor stage obtained from respectively (a) experimental pressure measurements, (b) steady-state calculations results and (c) unsteady calculations. It is plotted as a function of the stage setting ratio, such as points at the same abscissa can be compared. Numerical performances are computed using pressure values resulting of arithmetical averaging over all the pressure values probed at the exactly same locations as the experimental holes, distributed over the circumference on the hub and shroud walls.

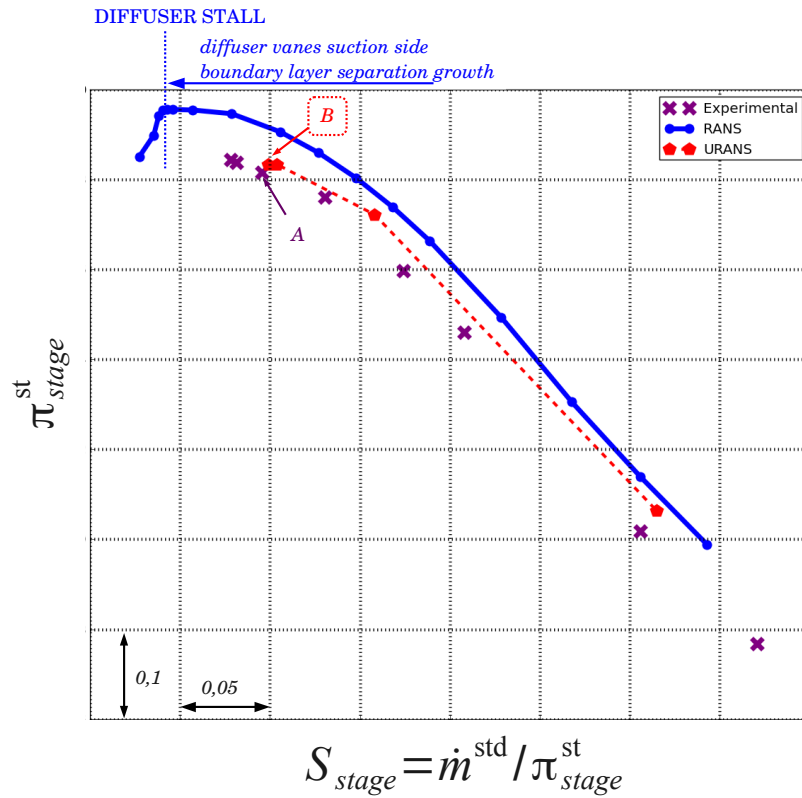


**Fig. 3: Total-to-static pressure ratio of the compressor stage**

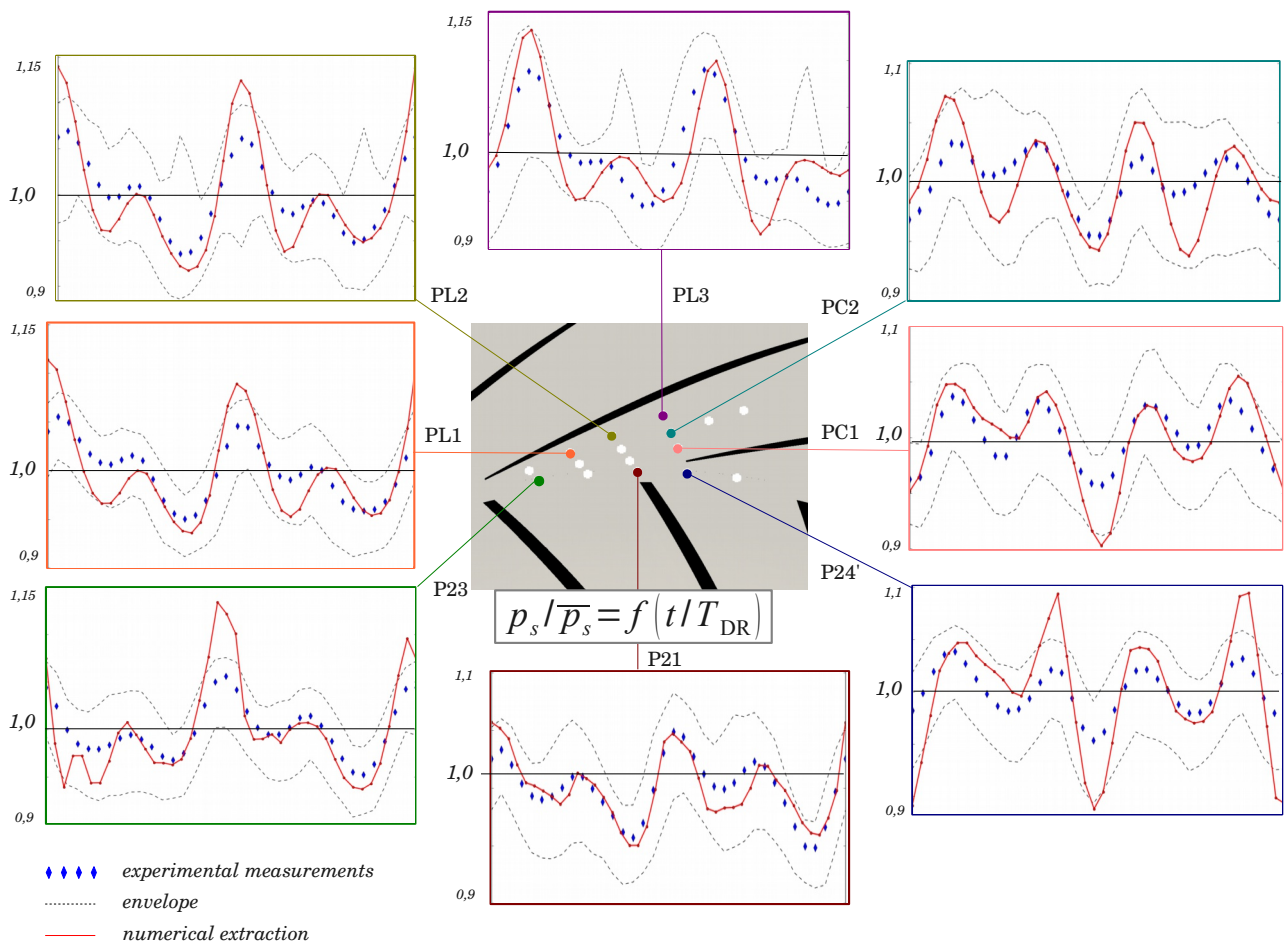


**Fig. 4: Static pressure variations at sensors locations on the shroud wall. Comparison between URANS and experimental results.**

A better correspondence with the experiments is clearly obtained with the unsteady calculations, compared to the steady-state results that predict stall-free operating points for setup ratios much lower and with excessively high total-to-static pressure ratio. URANS curve fits better to the experimental one, and predicts better the total-to-static pressure ratio saturation. The analysis of the RANS results have shown that this saturation is due to the growth of the boundary layer separation in the corner between the hub surface and the vane suction-side.

In order to reinforce the good adequacy of the time-dependent flow field issued from the URANS calculations, unsteady pressure signals are also compared between the two operating points labeled as *A* and *B* in Fig. 3. Experimental unsteady pressure signals at various locations over one diffuser period are shown Fig. 4. They result of an averaging over 100 impeller revolutions, sample frequency being equal to 35 times the BPF. The dashed line represent the extreme recorded values. Regarding the numerical pressure signals, they result of an extraction from the URANS flow field of the instantaneous pressure value at the sensors locations on the shroud wall.

The pressure fluctuations extracted from the URANS calculation are in very good agreement with the experiments. The amplitude of the peak is over-estimated for the P23 sensor for example, but the relative positions of peaks are correct, as their relative amplitudes. Note that four high pressure peaks are distributed over the diffuser period. They can be explained by the propagation of pressure waves generated by the passing of impeller blade in front of the diffuser vanes leading edges. These pressure waves will be shown in Fig. 6.

Considering the agreement between URANS numerical flow field and the experimental data, a detailed analysis of the flow behavior within the diffuser stage can be carried out with confidence in the validity of the numerical data. In particular, the temporal behavior of the hub-vane suction side corner boundary layer separation is studied in the next section.

## **TEMPORAL BEHAVIOR OF DIFFUSER BOUNDARY LAYER SEPARATION**

The skin-friction field is a marker of the interaction between the fluid and the solid, that allows a precise description of the flow structures and the tracking of boundary layer separations. Several evidences of the relevancy of skin-friction analysis in the understanding of various flow structures are given by Détery (2009). Principles of the skin-friction pattern analysis are well established for steady-state flow field, and criteria based on the study of the singularities and the strength of the skin-friction lines convergence allow to detect the onset of separations and their locations.

It becomes much more complex in case of unsteady flows. In particular, the instantaneous skin-friction pattern can be free of any singular points, in spite of the fact that fluid continuously separates from the solid wall (Jacobs *et al.*, 2007; Weldon *et al.*, 2008). The interpretation of skin-friction pattern in terms of flow structure should then be carefully conducted, and is the subject of research studies in progress (Haller, 2004; Peacock *et al.*, 2005; Surana *et al.*, 2008; Weldon *et al.*, 2008). Recently, Surana *et al.* (2008) have investigated the case of flow separations in periodic flows. They analyzed the separation from a Lagrangian point of view, as the ejection of fluid particles along particular geometric surfaces called “material surfaces”. After mathematical development, they concluded that in a flow that fluctuates around a steady averaged state, the fluid particles separate from the wall at a fixed location, stabilized thanks to the effect of the no-slip condition at walls and recognizable thanks to the analysis of the time-averaged skin-friction pattern instead of the instantaneous skin-friction patterns. They qualified such a type of separation as “fixed unsteady separation”. For that type of separations, the study of the instantaneous skin-friction patterns can lead to incorrect conclusions about the separation location.

Experimental investigations of a low Reynolds number flow around an oscillating and rotating cylinder have confirmed the previous conclusion about fixed unsteady separations for a wide range of problem parameters (Weldon, 2008). But some limitations were also enlighten: when the motion of the cylinder from side-to-side is very slow, the material spike follows precisely the cylinder motion. The separation then becomes a so-called “moving separation”. On the contrary, when the

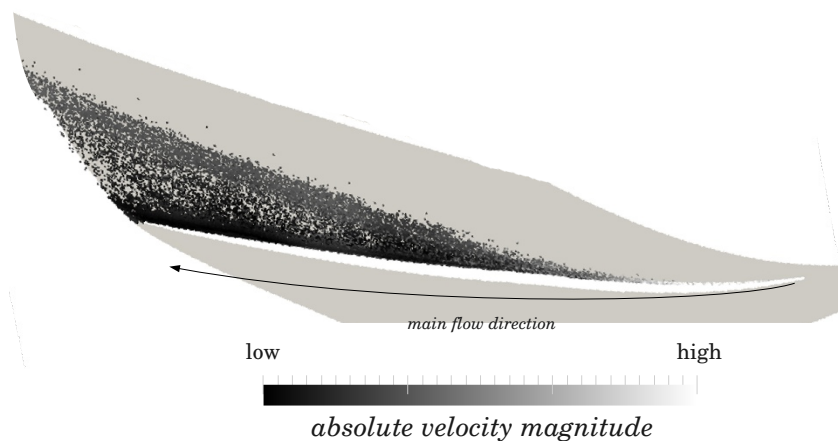
motion of the cylinder is set to very fast, no material spike is observed, and it becomes difficult to identify a location for the separation. Moreover, these experiments were conducted at a low Reynolds number, and extension to high Reynolds number flows remains uncertain, in particular due to the effect of high turbulence rate. For a flow behind a backward-facing step at a higher Reynolds number, driving a periodic shedding of a three-vortex system, Jacobs (2007) observed that the strong turbulent flow fluctuations in the corner area were altering the expected fixed unsteady separation into a moving separation. By studying the response of inertial particles, he also highlighted the link between the particle response time and the characteristic flow time, that may be considered in order to predict if the unsteady separation is fixed or moving.

In fact, the growth of either a fixed separation or an unsteady separation seems to be dependent of a number of parameters, including the characteristic times of external flow field variations and pressure waves scrolling, compared to the response time of the separation flow structure, that relies at least on the velocity of the fluid particle ejection, the instantaneous mass flow rate implied in the separation and the turbulence rate in the boundary layer. Then, an a priori determination of the nature of an unsteady separation is a difficult task.

A boundary layer separation was highlighted in the vaned diffuser thanks to steady-state simulation results and time-averaged URANS flow field (Marsan *et al.*, 2012). The present study aims at determining if this separation is either a fixed or a moving separation. This determination is not trivial given both the strong periodicity of the flow field, the high rate of turbulence and the high flow angle variations at the diffuser inlet. The conclusion will be decisive for the development of an efficient control strategy.

The following focuses on the study of the flow field in the diffuser for the operating point labeled “B” in Fig. 3. The evolution of the instantaneous skin-friction pattern is exposed, and linked to the pressure waves propagation created by the moving of the impeller blades in front of the diffuser vanes. Significance of that instantaneous skin-friction is investigated thanks to fluid particles tracking, that are numerically observable and constitute an unquestionable way for studying unsteady flow behavior.

Fig. 5 results of a fluid particles seeding from a surface close to the suction side of the diffuser vane. Fluid particles are periodically injected on points distributed over all the suction side, and then convected by the velocity vector field. The time step used for integration is  $1.10^{-6}$  seconds. The time corresponding to the snapshot shown in Fig. 5 is around  $7.10^{-3}$  seconds. It clearly highlights the occurrence of boundary separation, accordingly to the Prandtl definition as the ejection of fluid particles from the vicinity of the wall. A large low momentum flow area spreads across the diffuser passage, and results in both an increase in losses and a decrease in the diffusion level achievable by the diffuser.



**suction side.**

Fig. 6 highlights the temporal behavior of that separation. Only a half diffuser period is represented, the conclusions being qualitatively the same during the second period which corresponds to the splitter blade passage.

Fluid particles moving with a velocity magnitude smaller than 10 percent of the external flow velocity magnitude have been extracted from the fluid particles given in Fig. 5. The number of fluid particles plotted is then not constant, and the low momentum flow area thus observed is continuously fed with new fluid particles coming from upper span. Instantaneous skin-friction lines have also been plotted on the suction surface of the diffuser vanes thanks to a line integral convolution technique available in the open-source visualization software Paraview. More details about this technique are given in Sundquist (2001). For clarity, some of the skin-friction lines are superimposed in order to facilitate the interpretation and the understanding of the skin-friction topology. High values of static pressure are also superimposed in white, in order to link the temporal evolution of the skin-friction pattern to the impeller-diffuser interaction.

The skin-friction pattern analysis shows a periodical vortex shedding, driven by the high pressure gradient propagation. The vortices always originate from a fixed location at the hub-suction side corner, but are periodically convected by the pressure waves towards downstream. At the first in Fig. 6, the main corner vortex splits into two vortices, one of them being convected by the pressure wave. During the half period, two high pressure waves are observed, in spite of the fact that only one impeller blade passes in front of the diffuser vane. The  $\alpha_1$  high pressure wave is engendered by the interaction between the impeller blade currently passing in front of the observed diffuser vane, whereas the  $\alpha_2$  wave is created by the interaction between the previous impeller blade and the adjacent diffuser vane (in the direction opposite to the rotation).  $\alpha_2$  is then weaker than  $\alpha_1$  when reaching the suction side of the observed vane, as shown through the difference in the amplitudes of the four pressure peaks distributed over the diffuser period shown in Fig. 4. That explains the fact that the vortex does not split when  $\alpha_2$  passes. In case of transonic radial vaned diffusers, similar wave patterns have been described by Trébinjac *et al.* (2011).

Thus, it appears that the skin-friction topology is strongly affected by the impeller moving. However, it has to be interpreted with caution. In particular, the study of the fluid particles behavior does not reveal any formation of material vortices, in a sense of a rolling of particles trajectories. The vortex shedding actually corresponds to the propagation of a high vorticity value. But the speed of the vorticity propagation, that is the pressure wave propagation speed i.e. the speed of sound, is much higher than the velocity of the particles included in the low-momentum area. The pictures in Fig. 6 on the right hand column shows that low-momentum fluid particles in the corner are barely affected by the high pressure waves passage. There is no break-down of the low-momentum flow zone due to the passage of the pressure waves and the unsteadiness of the flow at diffuser inlet. A close examination of the trajectory of these low velocity particles shows more precisely that the passage of the pressure waves results only in a vibration of the particles around their main trajectories which are completely determined by the time-averaged flow field. Then, the separation is a so-called “fixed unsteady separation”, in accordance of the conclusion of Surana *et al.* (2008) about unsteady separations in periodic flows. The separation location is constant, even if the separation surface shape changes in time, and is correctly extracted from the time-averaged skin-friction pattern (Fig. 7). In this case, the low magnitude of flow velocity in the corner stabilizes the separation, and acts as the no-slip condition that was used by Surana in order to demonstrate the fixity of separations in unsteady flows with steady means.

On the other hand, Fig. 6 also exposes the variation of the extension of the low-momentum flow area due to the passage of the pressure waves. The singular instant shown Fig. 8 puts into evidence that variation. Particles near the low-momentum corner flow are periodically slow down by the high adverse pressure gradient, and enlarge the low-momentum flow zone. The steady-state calculations are obviously unable to render this time-dependent process. That results in significant differences between the extent of the separation predicted by the steady and the unsteady models. Fig. 7

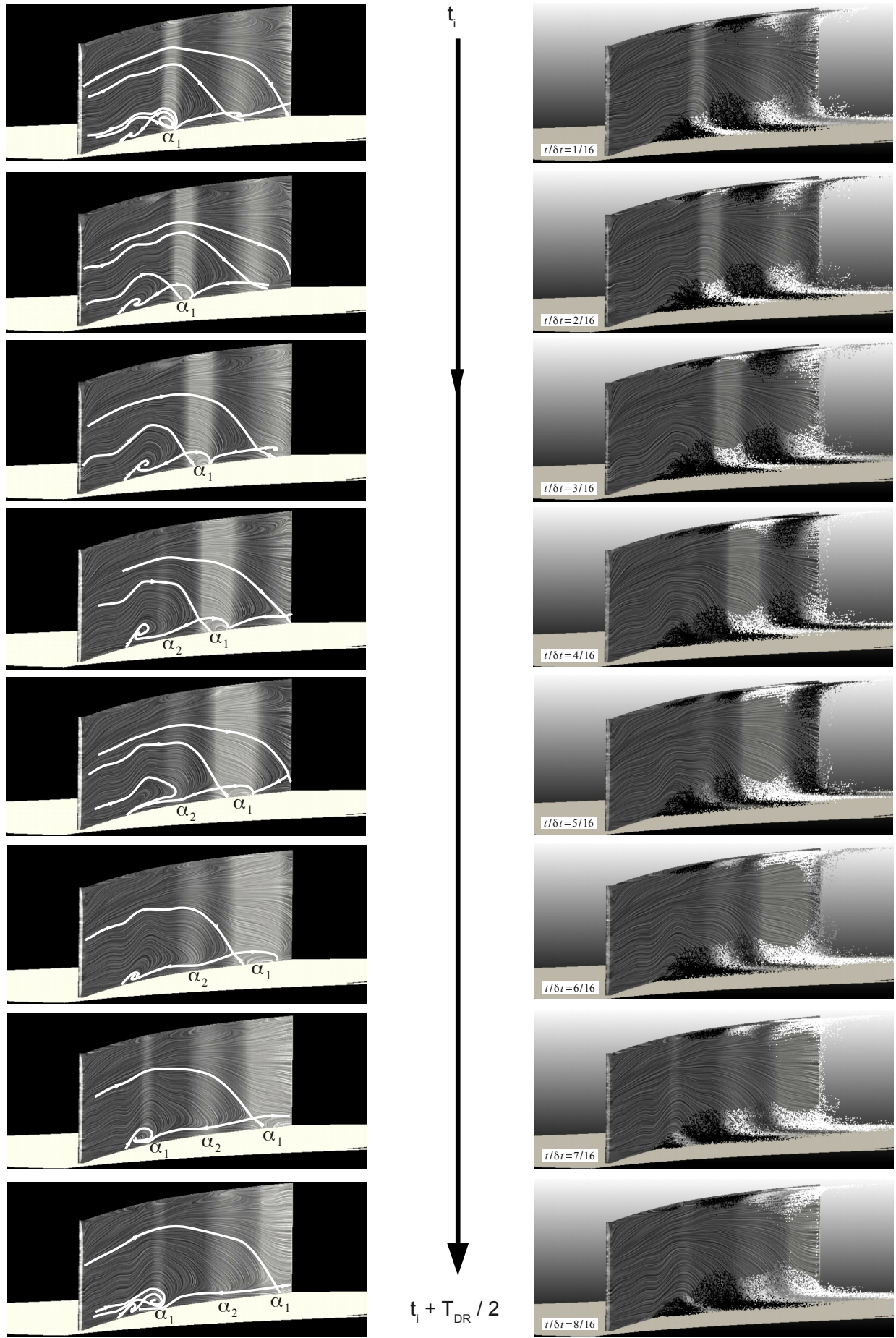


**Fig. 6: Temporal evolution of the diffuser boundary layer separation. Low-momentum flow particles. High static pressure is superimposed in white**

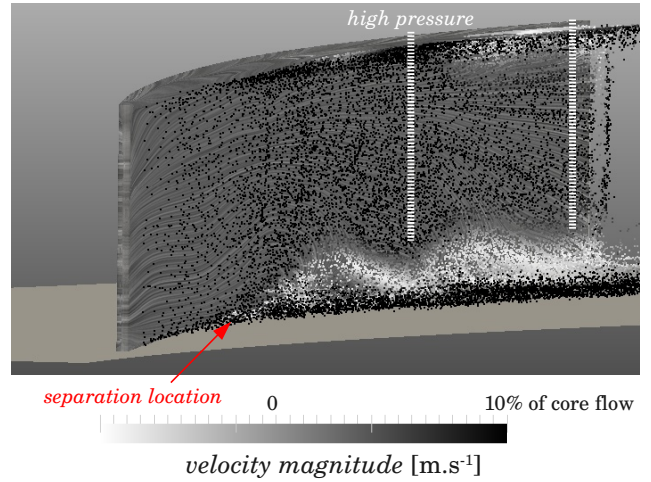
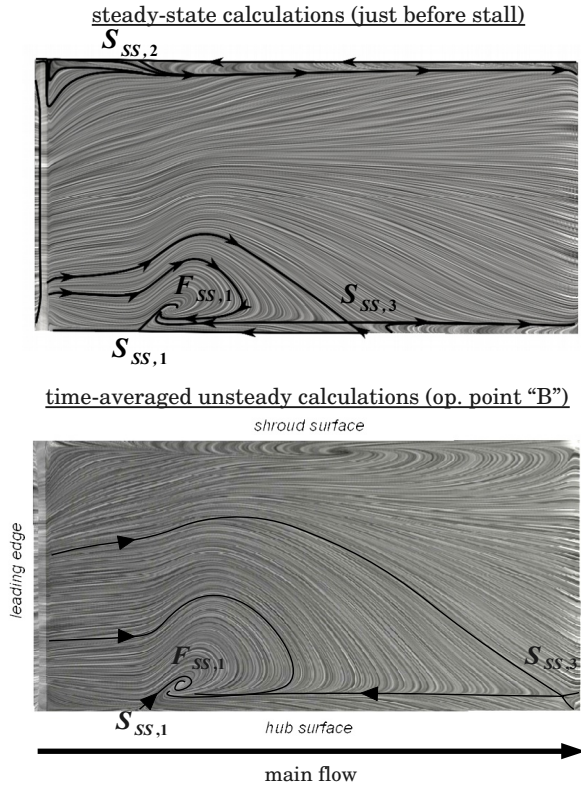


**Fig. 8: Effect of pressure waves on the low-momentum zone extent**

**Fig. 7: Steady and time-averaged skin-friction patterns on the suction side**

exposes a comparison between the steady and time-averaged skin-friction patterns on the vane suction side. The seed  $S_{SS,3}$  is located far downstream in the case of unsteady simulations, and the separated area on the suction side is enlarged.

However, the topology of the separation predicted by both simulations is the same. Above all, the seed  $S_{SS,1}$  that marks the separation location and is the key element for the development of a control strategy, is predicted at the same location.

## CONCLUSIONS

The present study of the temporal behavior of a boundary layer separation in a transonic radial vaned diffuser operating near surge has led to the significant non trivial conclusion that the separation is a “fixed unsteady separation”, according to the terminology introduced by Haller, Surana and collaborators (Surana *et al.*, 2008). The extent of the low-momentum flow area evolves in time, under the effect of the high pressure waves propagation, but the separation location remains constant and fluid particles trajectories in the separated zone are correctly described by the time-averaged flow field.

The second conclusion concerns the validity of RANS simulations. The topology of the separation predicted by the URANS simulations is the same as the one already observed in steady-state simulations. Moreover, and even if the extent of the low-momentum flow zone differs, the separation is predicted at the same location by both numerical models. The choice of the location of a suction slot aiming at controlling the separation seems then not affected by unsteadiness, and can be properly determined by steady-state flow analysis.

In further work, the aspiration strategy that was already tested with success in steady-state simulations by Marsan *et al.* (2012) will be implemented in phase-lagged calculations in order to confirm that conclusion, and the effective operating range enlargement resulting from the control of the hub-suction side corner separation.

Fillets should also be included in the numerical modeling in order to analyze their influence on the separation pattern, since sharp corner predetermine a separating line in the skin-friction pattern and could significantly modify the separation structure.

Lastly, if boundary layer suction technique is confirmed by the URANS simulations as an effective way for extending the compressor operating range, an experimental campaign should be conducted.

## ACKNOWLEDGMENTS

The authors would like to thank Turbomeca, Safran group, which supports the current study. ONERA, that provides the numerical code, and the *Agence Nationale de la Recherche et de la Technologie* that promotes the collaboration between research laboratories and industrialists.

Thanks also to Nicolas Bulot, aerodynamic engineer at Turbomeca, for his valuable support and the many talks all along the present PhD work, and Antoine Godard for his precious insights into flow separation and control.

The authors also would like to thank N. Garcia-Rosa from the DAEP, ISAE for providing the experimental datas.

## REFERENCES

- Bulot, Nicolas. 2010. "Analyse expérimentale et modélisation numérique des mécanismes d'interactions instationnaires à proximité du pompage d'un étage de compresseur centrifuge à fort taux de compression". PhD Thesis, 2010-06, Ecole Centrale de Lyon, LMFA, France.
- Came, PM. 1977. "The Current State of Research and Design in High Pressure Ratio Centrifugal Compressors". Aeronautical Research Council Current Papers ARC/CP-1363.
- Délery, Jean. 2009. "Décollement en écoulement tridimensionnel : points singuliers, lignes séparatrices et tourbillons". ONERA, the French Aerospace Lab.  
<http://www.ONERA.fr/conferences/decollement3d/>.
- Domercq, O. 1998. "Analyse Expérimentale Et Modélisation Des Interactions Rotor-stator Dans Les Compresseurs Centrifuges". Ecole Nationale Supérieure de l'Aéronautique et de l'Espace, Toulouse, France.
- Haller, G. 2004. "Exact Theory of Unsteady Separation for Two-dimensional Flows." *Journal of Fluid Mechanics* 512 (July). doi:10.1017/S0022112004009929.  
[http://www.journals.cambridge.org/abstract\\_S0022112004009929](http://www.journals.cambridge.org/abstract_S0022112004009929).
- Hill, R.A. 2007. "Simulation of spike stall inception in a radial vanted diffuser". Thesis, Massachusetts Institute of Technology. <http://dspace.mit.edu/handle/1721.1/42048>.
- Jacobs, G. B., 2007. "Inertial Particle Behavior in Unsteady Separated Flow." In *Bulletin of the American Physical Society*. Vol. Volume 52, Number 12. American Physical Society.  
<http://meetings.aps.org/link/BAPS.2007.DFD.FP.1>.
- Jacobs, G. B., A. Surana, T. Peacock, and G Haller. 2007. "Identification of Flow Separation in Three and Four Dimensions." In *45th AIAA Aerospace Sciences Meeting and Exhibit*. Aerospace Sciences Meetings. American Institute of Aeronautics and Astronautics.  
<http://dx.doi.org/10.2514/6.2007-401>.
- Kerrebrock, J.L. 2005. "Aspirated Compressors = Shorter, Lighter Engines: a Boon for Supercruising Jets." *Aero-Astro N°2*.  
<http://web.mit.edu/aeroastro/news/magazine/aeroastro-no2/2005kerbrock.html>.
- Leblanc, A. 2010. "Diffuser with enhanced surge margin."  
US Patent Number 20100077768.
- Marsan A., Trébinjac I., Coste S., and Leroy G., 2012. "Numerical Investigation of the Flow in a Radial Vaned Diffuser Without and with Aspiration." In *Proceedings of ASME Turbo Expo 2012, GT2012-68610*. Copenhagen, Denmark.

- Marsan A., Trebinjac I., Coste S., and Leroy G., 2012. “Study and Control of a Radial Vaned Diffuser Stall,” *International Journal of Rotating Machinery*, vol. 2012, Article ID 549048, 12 pages, 2012. doi:10.1155/2012/549048
- Neubauer, J. 2004. “Aérodynamique 3-D Instationnaire des Turbomachines Axiales Multi-étages”. PhD Thesis, Paris, France: Université Pierre et Marie Curie.
- Peacock, T., Coral, R., Haller, G., 2005. Experimental validation of the kinematic theory of unsteady separation, in: *AIAA Paper*. Presented at the 35th AIAA Fluid Dynamics Conference and Exhibit, AIAA, Toronto, Ontario Canada.
- Raw, J.A., 1986. Surge margin enhancement by a porous throat diffuser. *Canadian Aeronautics and Space Journal* 32, 54–61.
- Rochuon, N. 2007. “Analyse de l’écoulement tridimensionnel et instationnaire dans un compresseur centrifuge à fort taux de pression”. PhD Thesis, 2007-05, École Centrale de Lyon, LMFA, France.
- Schonenborn, H. 2001. “Removal of Cooling Air on the Suction Side of a Diffuser Vane of a Radial Compressor Stage of Gas Turbines.” US Patent Number 6210104.
- Sundquist, A. 2003. “Dynamic Line Integral Convolution for Visualizing Streamline Evolution.” *IEEE Transactions on Visualization and Computer Graphics* 9 (3) (September): 273 – 282. doi:10.1109/TVCG.2003.1207436.
- Surana A., Jacobs G., Grunberg O., and Haller G. 2008. “An Exact Theory of Three-dimensional Fixed Separation in Unsteady Flows.” *Physics of Fluids* 20 (10) (October 8): 107101–107101–22. doi:doi:10.1063/1.2988321.
- Trébinjac, I., N. Bulot, X. Ottavy, and Buffaz N. 2011. “Surge Inception in a Transonic Centrifugal Compressor Stage.” In *Proceedings of ASME Turbo Expo 2011*. GT2011-45116. Vancouver, British Columbia, Canada.
- Trébinjac I., Kulisa P., Bulot N., and Rochuon N. 2009. “Effect of Unsteadiness on the Performance of a Transonic Centrifugal Compressor Stage.” *Journal of Turbomachinery* 131 (4): 041011. doi:10.1115/1.3070575.
- Weldon, M., Peacock T., Jacobs G. B., Helu M., and Haller G. 2008. “Experimental and Numerical Investigation of the Kinematic Theory of Unsteady Separation.” *Journal of Fluid Mechanics* 611 (August 26). doi:10.1017/S0022112008002395. [http://www.journals.cambridge.org/abstract\\_S0022112008002395](http://www.journals.cambridge.org/abstract_S0022112008002395).